The International Journal of Advanced Manufacturing Technology (2024) 130:5199–5218
https://doi.org/10.1007/s00170-024-13009-9

ORIGINAL ARTICLE

An experimental assessment and optimisation of hole quality in Al2024-T3 aluminium alloy during abrasive water jet machining

Hang Shi[1] · Khaled Giasin[1] · Antigoni Barouni[1] · Zhongyi Zhang[1]

Received: 20 September 2023 / Accepted: 8 January 2024 / Published online: 23 January 2024

Abstract

Owing to its outstanding properties such as corrosion resistance, low density, relatively low cost, and stiffness, Al2024-T3 aluminium alloy has been widely applied in aircraft manufacturing. To perfectly assemble an aircraft, numerous high-quality holes are drilled into its structures employing conventional drilling processes. Conventional drilling poses some challenges such as thermal distortions, burr formations, and tool wear. Alternatively, abrasive water jet drilling (AWJD) is a thermal-free machining process that can be employed as an alternative to conventional drilling of aeronautical structures. Hence, in this work, the effect of abrasive water jet parameters, namely stand-off distance, water jet pressure, and abrasive mass flow rate, on hole-quality parameters was evaluated at traverse speed = 10 mm/min. Three parameters were stand-off distance = 1, 2, and 3 mm, abrasive mass flow rate = 200, 250, and 300 g/min, and water jet pressure = 1800, 2100, and 2600 bar. Using a 6 mm circular-movement diameter of the nozzle tip, optimal stand-off distance, water jet pressure, and abrasive mass flow rate obtained by multi-objective optimization were 2 mm, 250 g/min, and 2600 bar, respectively. The corresponding hole-quality parameters were Diameter = 6.232 mm, Kerf angle = 0.018°, Cylindricity = 0.051 mm, Perpendicularity = 0.033 mm, Circularity = 0.0041 mm and Surface roughness R_a = 2.909 µm. The results showed that water jet pressure had the greatest influence on Perpendicularity, Circularity; stand-off distance had the highest effect on Kerf angle; and abrasive mass flow rate has the largest influence on Hole diameter, Cylindricity and Surface roughness R_a, and R_z at the given value of traverse speed. The adopted optimization process for abrasive water jet of Al2024-T3 aluminium alloy was successfully verified through confirmation runs, clearly illustrating its benefits.

Keywords Hole-quality parameter · Machinability · Circular-motion diameter of nozzle tip · Al2024-T3 aluminium alloy · Abrasive waterjet drilling

Abbreviations

AMFR	Abrasive Mass Flow Rate (g/min)
AWJ	Abrasive Water Jet
AWJD	Abrasive Water Jet Drilling
CI	Confidence Interval
CMD	Circular-Motion Diameter (mm)
EDX	Energy-Dispersive X-ray
GRC	Grey Relational Coefficient
GRG	Grey Relational Grade
MD	Mechanical Drilling
SOD	Stand-Off Distance (mm)
S/N	Signal-to-Noise
TS	Traverse Speed (mm/min)
WJP	Water Jet Pressure
C_{yl}	Cylindricity (mm)
D	Diameter (mm)
D_{en}	Average diameter of a hole at the entry (mm)
D_{ex}	Average diameter of a hole at the exit (mm)
D_m	Average diameter of a hole at the middle (mm)
ΔD	Difference of diameters at the entry and exit (mm)
h	Thickness of Al2024-T3 aluminium alloy, $h = 8.0$ mm in the current work
H	Hole depth (mm)
K_f	Kerf angle (°)
$\max(x^0(p))$	Maximum value of parameter p measured in the current experiment

✉ Hang Shi
up969754@myport.ac.uk

✉ Khaled Giasin
khaled.giasin@port.ac.uk

[1] School of Mechanical and Design Engineering, University of Portsmouth, Portsmouth PO1 3DJ, UK

$\min(x^0(p))$	Minimum value of parameter p measured in the current experiment
n	Total number of measured data of a certain parameter p, or total number of measured data at a certain level of parameter p
O_b	Nominal value of diameter, $O_b = 6.000$ mm in the current work
p	A certain hole-quality parameter
P_{erp}	Perpendicularity (mm)
$\Delta_{0i}(p)$	Deviation sequence
R_a	Average surface roughness (µm)
R_e	Average roundness error (mm)
R_{em}	Roundness errors at the hole middle (mm)
R_{en}	Roundness errors at the hole entry (mm)
R_{ex}	Roundness error at the hole exit (mm)
R_z	Ten-point average surface roughness (µm)
S^2	Mean square error of a certain parameter at this level
T	Average value of this hole-quality parameter for all holes
T_{dof}	Total main factor degrees of freedom
V_2	Error of freedom degree
V_e	Error variance
$\overline{x}$	Average value of a given hole-quality parameter at a certain level
x_i	*i*Th value of this parameter
$x_i(p)$	*i*Th normalized value of parameter p
$x_i^0(p)$	*i*Th value of measured results
Y	Result predicted by single-objective optimization or by regression model
γ_i	Value of grey relational grade
Δ_{max}	Maximum value of deviation sequence
Δ_{min}	Minimum value of deviation sequence
ω_p	Weight factor of the pth hole-quality parameter
$\xi_i(p)$	Grey relational coefficient of the ith value of parameter p

1 Introduction

To assemble an aircraft, approximately 1.5 to 3.0 million holes requires drilling [1–3]. The diameters of these through-holes are usually from 4.8 to 10 mm [4, 5]. It has been reported that nearly 70% of fatigue failures in an aircraft body are from the poor assemble of its parts and nearly 80% of fatigue cracks are originated from poor quality holes [6, 7]. In order to solve the fatigue-failure and fatigue-crack problems, high-quality holes need to be drilled prior to the assembly of an aircraft. Al2024-T3 aluminium alloy is an important material employed in the production of aircrafts. In addition to manufacturing of fibre metal laminates (FMLs) like GLARE, CARALL, and ARALL [4, 8], it has been used to produce fuselage skin and wing sections [9, 10]. While there are numerous methods for drilling Al2024-T3 aluminium alloy, conventional drilling also known as mechanical drilling (MD) and AWJD are the most useful when it comes to producing holes in the manufacture of aircraft. [11]. High-quality holes in FML structures are difficult to obtain when using mechanical drills because the machinability of Al2024-T3 aluminium alloy is very different from that of S2/FM94 laminate due to the variation in thermal and mechanical properties, but this problem can be overcome by AWJ processing [12, 13]. However, as previously stated, only a handful of studies have been reported on AWJ drilling of Al2024-T3 aluminium alloy, let alone FMLs.

Numerous investigations on drilling of Al2024 aluminium alloys have been reported using the MD approach, as reviewed by Giasin et al. [9]. Nouari et al. [14, 15] and Davoudinejad et al. [16] drilled Al2024 aluminium alloy with HSS drills, WC–Co cemented carbide drills, and cemented tungsten carbide drills. They mainly studied the influence of MD parameters on the hole quality, tool wear, and tool life, summarised the wear mechanisms of drills; and obtained the optimal MD parameters. Kurt et al. [17, 18] drilled Al2024 alloy with coated and uncoated HSS drills, evaluated the influence of MD conditions on the hole quality, and optimised the MD parameters. Ralph et al. [10] and Elajrami et al. [19] studied the effect of pilot holes on the drilling quality of Al2024 alloy under different MD conditions. They found that pilot holes could effectively improve the hole-surface finish and K_f. Köklü [20] drilled Al2024, Al7070, and Al7050 aluminium alloys using high-speed-steel twist drills, investigated the influence of MD parameters on R_a and burr height, and optimized the MD parameters.

To improve the drilling quality, Amini et al.[21, 22]. added ultrasonic vibrations to the drilling process of Al2024 aluminium alloy. Compared to the ordinary drilling methods, they found that the ultrasonic drilling approach could effectively reduce thrust force and thus, improve the hole quality. Abdelhafeez et al. [23] drilled Al2024 aluminium alloy using solid WC twist drills and studied the influence of cutting speed and feed rate on R_e, burr parameter, and tool wear. High-quality R_e and deviation of D of the same hole were obtained. Giasin et al. [9] used carbide twist drills to drill Al2024 alloy and evaluated the influence of spindle speed and feed rate on the hole-quality parameters. They also used a finite-element model to predict the hole quality under the same condition. Good agreement was obtained between theory and experiment. Aamir et al. [24] drilled Al2024 aluminium alloy using twist drills and studied the influence of spindle speed and feed rate on certain hole-quality parameters. They concluded that multi-spindle simultaneous drilling could machine holes with high-quality R_e, P_{erp}, and C_{yl} without regard to drilling parameters.

Compared to numerous MD studies, only one group of AWJD work about Al2024 alloy is currently available in the literature [25], as commented in [26]. Including AWJD of all types of aluminium alloys, only seven groups of experimental studies have been found in the literature thus far [25, 27–32]. Cenac et al. [25] used nozzle size, *WJP*, *TS*, *AMFR*, and *H* as AWJD parameters to drill Al2024-T3 aluminium alloy. They proposed a model of optimal *AMFR* and established an analytical relationship between the optimal *AMFR* and *H*. Orbanic and Junkar [27] used AWJ to drill AlMg1SiCu alloy, studied the influence of cutting time on *H* and *D*, and evaluated the analytical relationship between the *D*, *H* and the cutting time. Using AWJ to drill Al6061 aluminium alloy, Akkurt [28] studied the influence of material thickness on drilling time and established an empirical equation used to predict *H* and *D* at different machining times. However, no hole-quality parameters were evaluated in these experimental studies [25, 27, 28].

Recently, Nyaboro et al. [29] simulated AWJD of Al7075-T6 aluminium alloy using CFD software and performed the AWJD trials to verify their simulated results. In detail, they used *WJP*, *SOD*, and machining time as AWJD parameters to study the material removal rate, diameter at the hole entrance, aspect ratio, kerf profile, and hole diameter. A favorite agreement was attained between the simulated results and the measurements. Lathif et al.[30]. studied the influence of *TS*, *SOD*, *AMFR*, and *WJP* on R_a when drilling Al7075 aluminium alloy; and developed a formula to predict R_a with enough accuracy in the given experimental range. Tekaüt [31] studied the effect of *TS* on R_e and C_{yl} when using AWJ to drill AA7075 aluminium alloy, displayed many images at the surface of hole entry and exit sides, and concluded that smaller *TS* could generate better C_{yl} and R_e. Ravi and Srinivasu [32] investigated the influence of *WJP*, *TS*, and *AMFR* on *D*, K_f, C_{yl}, R_e, *MRR*, and hole profile, observed surface morphology, damage region, burr formation, edge radius, and uncut material, and obtained several interesting conclusions.

As per the above-mentioned reviews, it is evident that the MD properties of Al2024 aluminium alloy have been studied to some extent in the open literature. Several hole-quality parameters such as *D* [9, 14–18, 23, 24], C_{yl} [24], R_e [9, 17, 23, 24], P_{erp} [24], R_a [9, 10, 14, 15, 17–20], and R_z, were measured; and K_f [10, 19] and ΔD were calculated. In contrast to these, only limited hole-quality parameters were measured when drilling various types of aluminium alloys with AWJ [29–32], let alone Al2024-T3. Furthermore, multi-objective optimization has not been done for all hole-quality parameters to date, even for holes drilled using MD approaches [9, 10, 14–29]. As a non-conventional drilling approach, AWJD has been extensively employed in various drilling processes due to its advantages such as small cutting force, versatility, no heat-affected zone, and flexibility [33]. According to the above-mentioned reviews, only four experimental groups have reported very few hole-quality parameters when using AWJ to drill various aluminium alloys [29–32]. Hence, AWJD is used to study the drilling machinability of Al2024-T3 aluminium alloy in this work. In addition, the results reported herein can provide useful guidelines when using AWJ to drill holes in FMLs.

2 Materials and methods

2.1 Materials, experimental setup, and experimental design

Al2024-T3 aluminium alloy plate was supplied by Dongguan Yida Metal Materials Co., LTD, China. Its dimensions are 160 mm in length, 160 mm in width, and 8 mm in height. Its percentage compositions are 90.7 – 94.7% aluminium, 3.4 – 4.9% copper, 1.2 – 1.8% magnesium, 0.3 – 0.9% manganese, 0.5% iron, 0.5% silicon, 0.25% titanium, 0.25% zinc, and 0.1% chromium [9]. Figure 1a shows the AWJD setup and workpiece. An aluminium alloy test coupon was fixed on the machine table. All holes were drilled by using the AWJD setup (iCUTwater, Germany), which was controlled by a computer. Figure 1b shows the AWJD path. The steps undertaken to perform the setup to drill holes is described briefly in previous work [34].

As *TS* has a great effect on R_e and C_{yl} of holes drilled through aluminium alloy with AWJ, it is very important to choose appropriate *TS* to perform high-quality drilling [31]. For this reason, a series of drilling tests were done only with the variation of *TS*. For *SOD* = 2 mm, *WJP* = 2100 bar, and *AMFR* = 200 g/min, visual inspection confirmed that C_{yl} and R_{ex} were bad when *TS* ≥ 50 mm/min and the edge surface finish of holes was very poor when *TS* exceeded 100 mm/min. When *TS* ≤ 30 mm/min, the edge surface finish of holes was visually satisfactory. Figure 2 illustrates the images at the entry and exit surfaces of the hole drilled with *TS* = 10 mm/min, *SOD* = 3 mm, *AMFR* = 300 g/min, and *WJP* = 2100 bar. From Fig. 2, one can clearly see that no burrs were formed on the hole edges at the entrance and exit sides. It is the reason why burr formation was not evaluated in this work.

It should be noted than drilling time was approximately 9.5 min for *TS* = 5 mm/min and 5.0 min for *TS* = 10 mm/min. Further inspection with CMM showed that the quality of holes drilled with *TS* = 5 and 10 mm/min was almost the same. Taking into account the drilling time and consumption of abrasives, *TS* was set as 10 mm/min in this experiment.

Three variable AWJD parameters were *AMFR*, *SOD*, and *WJP*. Each parameter had three levels, as listed in Table 1. *AMFR* in Table 1 was the value set by computer. Abrasive grits were 120# garnets. Figure 3 illustrates their SEM images and EDX spectroscopy. Abrasives hit the target zone

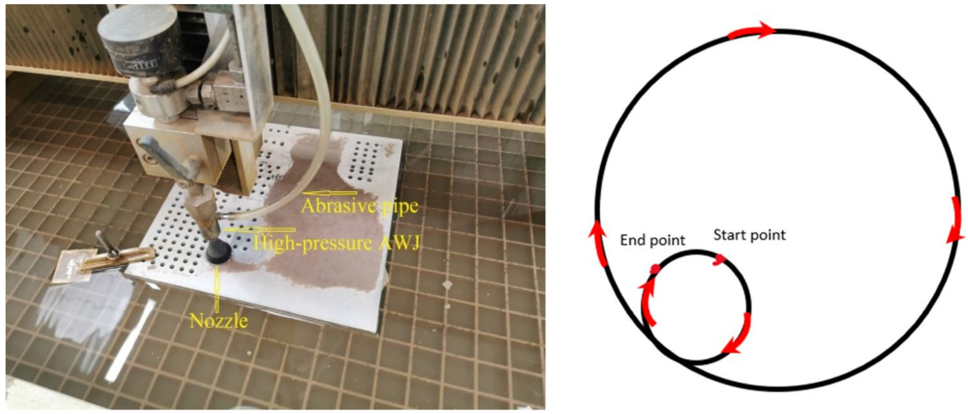

(a) (b)

Fig. 1 Diagrams of (**a**) AWJD experimental setup and workpiece and (**b**) AWJD path

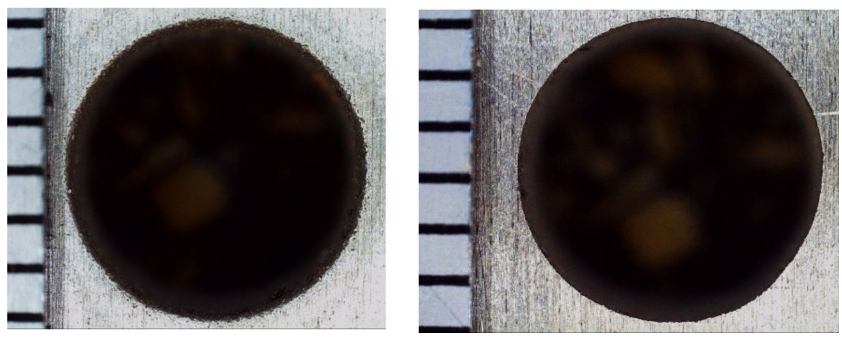

(a) (b)

Fig. 2 Images at (**a**) entry surface and (**b**) exit surface of a hole drilled with *SOD* = 3 mm, *WJP* = 2100 bar, and *AMFR* = 300 g/min

Table 1 AWJD parameters used for Al2024-T3 aluminium alloy

Variables	unit	Level 1	Level 2	Level 3
WJP	bar	1600	2100	2600
SOD	mm	1	2	3
AMFR	g/min	200	250	300
TS	mm/min	10	-	-

at an impingement angle of 90°. The nozzle was made of tungsten steel. The orifice diameter is 0.25 mm. *CMD* of the nozzle tip is 6.000 mm. The required diameter of holes was 6.000 mm. Based on the full factorial design of experiment, a total number of 27 holes were drilled.

2.2 Measurement of geometrical parameters D, ΔD, K_f, R_e, C_{yl}, and P_{erp} and measurement of R_a and R_z

Figure 4a shows a schematic diagram of Mitutoyo CMM (Crysta-Apex S) to measure the geometrical parameters, D, R_e, C_{yl}, and P_{erp}. To accurately determine the geometrical parameters, coordinate data were measured at the three positions (entry, middle, and exit) of each hole. D, R_e, C_{yl}, and P_{erp} of each hole were directly fitted using these coordinate data. The workpiece was tightly clamped on the CMM worktable. The convenience of CMM measurement was considered when designing the positions of the holes being drilled. As a result, CMM was able to continuously measure all required coordinate data of 27 holes without any interruption.

When coordinate data at the three locations were measured and D_{en}, D_m, and D_{ex} of the same hole were fitted, the average D was calculated according to [9]

$$D = \left(D_{en} + D_m + D_{ex}\right)/3 \tag{1}$$

ΔD of the same hole and was calculated by,

$$\Delta D = \left|D_m - D_{ex}\right|; \Delta D = \left|D_m - D_{ex}\right|; \text{ or } \Delta D = \left|D_{en} - D_{ex}\right| \tag{2}$$

Of these values, the largest one was regarded as the final ΔD and reported in this work. K_f was calculated with [19]

$$K_f = \arctan\left[\left(D_{ex} - D_{en}\right)/2h\right] \tag{3}$$

Similar to D, R_e was also calculated by averaging three values: R_{en}, R_{em}, and R_{ex}.

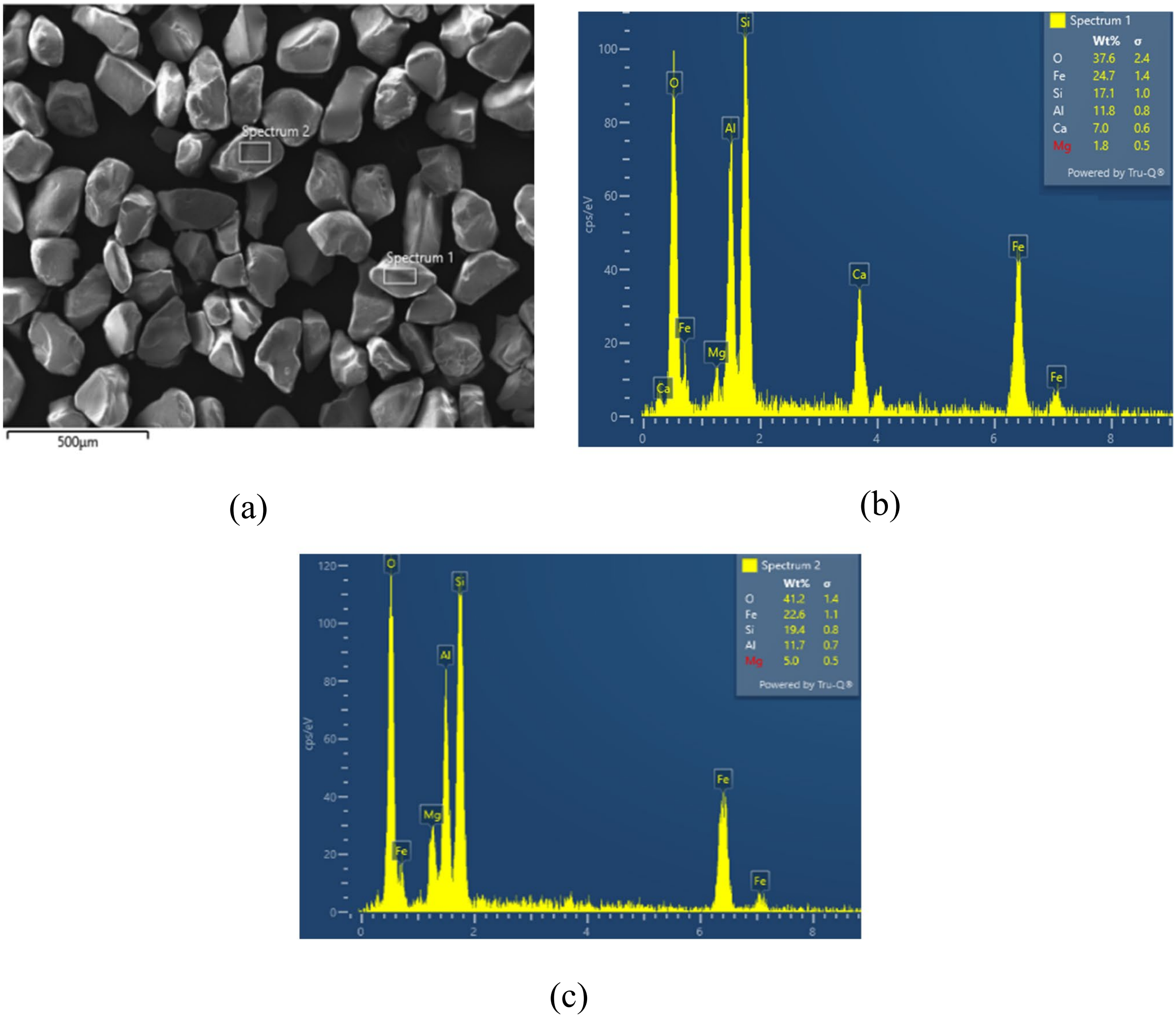

Fig. 3 120# garnets employed in the experiment: (**a**) SEM image, (**b**) and (**c**) EDX spectroscopy of abrasives 1 and 2

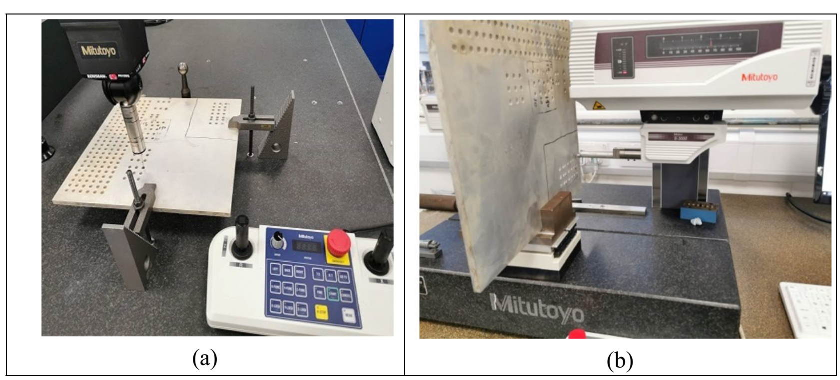

Fig. 4 Diagram to measure (**a**) coordinate data and (**b**) surface roughness of holes

Figure 4b shows the roughness tester (Mitutoyo S-3000, Japan) employed to measure surface roughness parameters. Only R_a and R_z were analysed in this work. To improve the measurement accuracy and experimental reliability, the surface roughness of each hole was measured along the four hole-axis directions (0°, 90°, 180°, and 270°). The mean value of the four directions represented the final R_a and R_z of each hole and was reported in this work.

2.3 Single-objective optimization based on Taguchi method

Single-objective optimization employs three approaches, smaller-is-better, nominal-is-better, and larger-is-better, to predict optimal drilling parameters [35]. Eight hole-quality parameters, D, ΔD, K_f, R_e, C_{yl}, P_{erp}, R_a, and R_z, were studied in this work. The smaller are ΔD, K_f, P_{erp}, C_{yl}, R_e, R_a, and R_z, the better the hole quality is, predicting that the smaller-is-better approach can be used to calculate the *S/N* ratio for these seven parameters. The closer the D is to the nominal value, the better the quality of drilled hole will be, showing that the nominal-is-better method can be employed to calculate the *S/N* ratio for D.

The smaller-is-better approach employed Eq. (4) to calculate the *S/N* ratio of a hole-quality parameter [35],

$$\frac{S}{N} = -10log(\frac{1}{n}\sum_{i=1}^{n} x_i^2) \tag{4}$$

The nominal-is-better approach employed Eq. (5) to calculate the *S/N* ratio [35],

$$\frac{S}{N} = 10log(\frac{\overline{x}}{S^2}) \tag{5}$$

The largest *S/N* corresponded to the optimal level of this drilling parameter. Three variable AWJD parameters were used in this work and each had three levels, as seen in Table 1. After determining the optimal level corresponding to the maximum *S/N* ratio, the optimal value of this hole-quality parameter could be predicted by [36]

$$Y = T + (A - T) + (B - T) + (C - T) \tag{6}$$

In Eq. (6), A, B, and C were the mean value of this parameter only at the corresponding optimal level. *CI* of the predicted value was computed based on [35]

$$CI = \sqrt{F_{\alpha,1,V_2} \bullet V_e \bullet (\frac{1}{n_{eff}} + \frac{1}{r})} \tag{7}$$

with

$$n_{eff} = \frac{T_{exp}}{1 + T_{dof}} \tag{8}$$

In Eqs. (7) and (8), $\alpha = 0.05$, $r = 1$, and $T_{exp} = 27$ in this work. V_2, V_e and T_{dof} were given by ANOVA.

2.4 Multi-objective optimization based on Taguchi method

Multi-objective optimization is employed to determine the optimum values of more than one hole-quality parameter simultaneously. The following is a brief introduction to multi-objective optimization of *WJP*, *SOD*, and *AMFR* for D, ΔD, K_f, R_e, C_{yl}, P_{erp}, R_a, and R_z.

2.5 Normalization of experimental results

Different hole-quality parameters may possess different physical units, resulting in difficult comparisons between them. In this work, the unit of D, ΔD, R_e, P_{erp}, and C_{yl} is mm; and K_f is in degree; while the unit of R_a and R_z is μm. These parameters must be normalized to be dimensionless to calculate the GRCs [35, 36]. Seven smaller-is-better parameters, ΔD, C_{yl}, R_e, K_f, R_a, R_z and P_{erp}, were normalized with [35, 36]

$$x_i(p) = \frac{\max(x_i^0(p)) - x_i^0(p))}{max(x^0(p)) - min(x^0(p))} \tag{9}$$

One nominal-is-better hole-quality parameters, D, was normalized as per [35]

$$x_i(p) = \frac{\left|x_i^0(p) - O_b\right|}{max[max(x_i^0(p)) - O_b, O_b - min(x_i^0(p))]} \tag{10}$$

2.6 Calculation, determination and ranking of GRC

$\xi_i(p)$ was calculated by [35, 36]

$$\xi_i(p) = \frac{\Delta_{min} + \zeta\Delta_{\max}}{\Delta_{0i} + \zeta\Delta_{\max}} \tag{11}$$

Here, $\Delta_{0i}(p)$ was determined with

$$\Delta_{0i}(p) = \left|x_i(p) - 1\right| \tag{12}$$

In Eqs. (11) and (12), ζ was 0.5; $x_i(p)$ was calculated by Eq. (9) or (10).

γ_i in a grey system was calculated by [35, 36]

$$\gamma_i = \sum_{p=1}^{n} \omega_p \xi_i(p) \tag{13}$$

Here, $n = 8$ was the total number used for multi-objective optimisation. ω_p should meet the following equation,

$$\sum_{p=1}^{n}\omega_p = 1 \quad (14)$$

Assuming that the weight factor of each hole-quality parameter was the same, Eq. (13) could be simplified as [35, 36]

$$\gamma_i = \frac{1}{n}\sum_{p=1}^{n}\xi_i(p) \quad (15)$$

GRG values were ranked in order from the smallest to the largest, with the highest order corresponding to the optimal AWJD parameters. The hole quality was optimal when holes were drilled with the optimum AWJD parameters.

3 Results and discussion

3.1 Effect of AWJD parameters on *D*, Δ*D*, and K_f

Tables 2 and 3 gives D_{en}, D_m, D_{ex}, D, ΔD, K_f, R_{en}, R_{em}, R_{ex}, C_{yl}, R_e, P_{erp}, R_a, and R_z of 27 holes drilled with all possible combinations of *WJP*, *SOD*, and *AMFR*. It can be observed from Table 2 that D_{en}, D_m, and D_{ex} increase with an increase of *AMFR* at the same *WJP* and *SOD* without exception. This change rule can be explained by the fact that: the greater the *AMFR*, the more the abrasives with material removal ability in unit volume of AWJ beam, and the more abrasives with material removal ability arrive at the target unit area per unit time and therefore, the more material could be removed from the target zone, resulting in large D_{en}, D_m, and D_{ex}.

Similar to D_{en}, D_m, and D_{ex} increasing with *AMFR*, the three parameters increase with *WJP* when keeping *SOD* and *AMFR* invariable. This can be explained due to the kinetic energy of abrasives increasing with *WJP*, naturally increasing the effective material removal ability of abrasives.

In the current experiment, on one hand, if *TS* was small enough, a sufficient number of abrasives with material removal ability arrived at the target unit area in unit time, resulting in observable material removal. On the other hand, if *TS* was large enough, only a small number of abrasives in the outer area with large kinetic energy arrived at the target unit area in unit time compared to small *TS*. Proper material

Table 2 Experimental values for D_{en}, D_m, D_{ex}, D, ΔD, and K_f

Hole	*SOD*	*WJP*	*AMFR*	D_{en}	D_m	D_{ex}	D	ΔD	K_f
No	(mm)	(bar)	(g/min)	(mm)	(mm)	(mm)	(mm)	(mm)	(°)
1	1	1600	200	6.098	6.068	6.071	6.079	0.003	0.097
2	1	1600	250	6.116	6.121	6.117	6.118	0.005	0.004
3	1	1600	300	6.144	6.147	6.142	6.144	0.005	0.007
4	1	2100	200	6.103	6.118	6.107	6.109	0.015	0.014
5	1	2100	250	6.119	6.133	6.145	6.132	0.026	0.093
6	1	2100	300	6.166	6.183	6.182	6.177	0.017	0.057
7	1	2600	200	6.130	6.131	6.136	6.132	0.006	0.021
8	1	2600	250	6.124	6.143	6.165	6.144	0.041	0.147
9	1	2600	300	6.164	6.175	6.198	6.179	0.034	0.122
10	2	1600	200	6.094	6.068	6.070	6.077	0.026	0.086
11	2	1600	250	6.025	6.123	6.116	6.088	0.098	0.326
12	2	1600	300	6.159	6.154	6.150	6.154	0.009	0.032
13	2	2100	200	6.098	6.098	6.093	6.096	0.005	0.018
14	2	2100	250	6.125	6.145	6.139	6.136	0.020	0.050
15	2	2100	300	6.156	6.184	6.174	6.171	0.028	0.064
16	2	2600	200	6.137	6.142	6.141	6.140	0.005	0.014
17	2	2600	250	6.162	6.169	6.170	6.167	0.008	0.029
18	2	2600	300	6.173	6.186	6.205	6.188	0.032	0.115
19	3	1600	200	6.150	6.122	6.083	6.118	0.067	0.240
20	3	1600	250	6.189	6.168	6.147	6.168	0.042	0.150
21	3	1600	300	6.209	6.186	6.183	6.193	0.026	0.093
22	3	2100	200	6.154	6.150	6.137	6.147	0.008	0.061
23	3	2100	250	6.204	6.189	6.185	6.193	0.019	0.068
24	3	2100	300	6.216	6.232	6.231	6.226	0.016	0.054
25	3	2600	200	6.170	6.160	6.154	6.161	0.016	0.057
26	3	2600	250	6.194	6.193	6.202	6.196	0.009	0.029
27	3	2600	300	6.228	6.234	6.233	6.232	0.006	0.018

Table 3 Experimental results for R_{en}, R_{em}, R_{ex}, C_{yl}, R_e, P_{erp}, R_a, and R_z results as well as their multi-objective optimization analysis

Hole	R_{en}	R_{em}	R_{ex}	C_{yl}	R_e	P_{erp}	R_a	R_z	GRG	Ranking
No	(mm)	(mm)	(mm)	(mm)	(mm)	(mm)	(μm)	(μm)		
1	0.033	0.059	0.086	0.090	0.059	0.285	3.289	27.614	0.5537	6
2	0.029	0.050	0.073	0.073	0.051	0.160	3.144	26.313	0.6695	17
3	0.032	0.056	0.080	0.074	0.056	0.133	3.138	25.947	0.6928	20
4	0.039	0.036	0.074	0.055	0.050	0.078	3.483	26.756	0.6478	13
5	0.030	0.034	0.045	0.049	0.036	0.099	3.424	28.044	0.6026	11
6	0.025	0.044	0.057	0.065	0.042	0.065	2.832	28.124	0.7180	22
7	0.027	0.041	0.063	0.064	0.044	0.078	3.299	29.995	0.6508	15
8	0.026	0.027	0.041	0.073	0.031	0.037	2.915	23.727	0.6796	23
9	0.023	0.054	0.052	0.070	0.043	0.109	2.876	25.488	0.6759	18
10	0.043	0.075	0.071	0.078	0.063	0.290	3.161	27.890	0.5326	4
11	0.130	0.051	0.065	0.130	0.082	0.721	3.345	27.690	0.3773	1
12	0.025	0.047	0.057	0.057	0.043	0.265	3.026	30.196	0.6488	14
13	0.036	0.060	0.060	0.060	0.052	0.278	3.098	25.007	0.6684	19
14	0.042	0.040	0.066	0.075	0.049	0.271	2.992	28.959	0.5996	9
15	0.037	0.050	0.054	0.064	0.047	0.022	2.935	24.038	0.7416	24
16	0.031	0.046	0.063	0.062	0.047	0.024	3.307	26.516	0.7060	21
17	0.023	0.043	0.056	0.051	0.041	0.023	2.909	26.480	0.7721	27
18	0.026	0.043	0.045	0.079	0.038	0.171	3.297	25.949	0.6125	10
19	0.034	0.063	0.102	0.102	0.066	0.132	3.687	29.864	0.4498	2
20	0.035	0.054	0.100	0.100	0.063	0.168	3.418	25.041	0.5658	5
21	0.031	0.074	0.081	0.081	0.062	0.255	3.274	26.246	0.6179	7
22	0.044	0.057	0.075	0.075	0.059	0.186	3.591	27.599	0.5997	8
23	0.033	0.074	0.069	0.084	0.059	0.121	3.214	24.785	0.6840	12
24	0.022	0.027	0.039	0.050	0.029	0.195	3.406	29.340	0.7408	25
25	0.049	0.060	0.102	0.102	0.070	0.144	3.808	31.987	0.5586	3
26	0.035	0.065	0.062	0.073	0.054	0.242	3.214	26.009	0.6952	16
27	0.024	0.050	0.061	0.057	0.045	0.193	3.078	27.156	0.8073	26

removal was difficult since only a small number of abrasives had sufficient material removal ability via their kinetic energy. It may be the reason why poor quality of holes was observed at high *TS*.

TS was small and *AMFR* was large, suggesting that numerous abrasives hit the target unit area per unit time. Although the proportion of abrasives with effective material removal ability in the outer region of AWJ was small, due to a large number of abrasives arriving at the machining zone in unit time, numerous abrasives could effectively remove the material from the target zone. Table 2 shows that a reduction of *AMFR* and/or *WJP* can bring D_{en}, D_m, and D_{ex} closer to the required value. The reason is that the total amount of abrasives with effective material removal power was reduced by reduction of *AMFR* and/or *WJP*. Table 2 also shows that all D_{en}, D_m, and D_{ex} were larger than the required D, indicating that adjusting *CMD* to an appropriate value might be an effective approach to make D and C_{yl} very close to 6.000 mm.

The influence of abrasives in the outer area on the hole diameter can be evaluated by comparing D_{en}, D_m, and D_{ex} of the same hole. Table 2 shows that D_m is usually large compared to D_{en} and D_{ex}. The reason is probably twofold. One is that the dimension of the AWJ beam expands with the forward motion [29]. The other is owing to secondary erosion by broken abrasives bouncing back from the blind-hole bottom [37, 38]. Ravi and Srinivasu [32] reported that D decreased with increasing H, different from the change rule reported in the current work.

The distances from the nozzle tip to the top and middle of each hole were 2 and 6 mm for $SOD = 2$ mm, and 3 and 7 mm for $SOD = 3$ mm, respectively. AWJ expanded with an increase in transmission distance [29], indicating that the material removal ability of abrasives in the outer area of AWJ became weak or even lost due to the reduction of kinetic energy [38]. Although the abrasives with material removal power in the outer area had a low concentration, for very small *TS*, abrasives with effective material removal power were still enough since the total amount of abrasives arriving at the target unit area in unit time was enormous, thus resulting in relatively large D_m as *SOD* increased.

The above conclusion is reinforced by the variation of D_{en} with *SOD* at the same *AMFR* and *WJP*. For example, when *WJP* = 2600 bar and *SOD* = 1, 2, and 3 mm, the D_{en} values are 6.130, 6.137, and 6.170 mm for *AMFR* = 200 g/min, respectively; those are 6.124, 6,162, and 6.194 mm for *AMFR* = 250 g/min, respectively; and those are 6.164, 6.173, and 6.228 mm for *AMFR* = 300 g/min, respectively. The largest D_{en} is 6.228 mm, which is located at *SOD* = 3 mm, *WJP* = 2600 bar, and *AMFR* = 300 g/min. D_{en} does not increase greatly when *SOD* increases from 1 to 2 mm. The reason might be that the AWJ expansion is not obvious in such a short distance. In the drilling trials, this phenomenon was not obvious at high traverse speeds such as *TS* = 150 mm/min, when keeping *WJP* and *AMFR* constant. Nyaboro et al.[29]. reported that D_{en} of Al7075-T6 aluminium alloy increased with *SOD* and *WJP* when they simulated AWJD employing CFD. The present experimental results compare favorably with those simulated by Nyaboro et al. [29].

After passing through the middle section of the hole, AWJ continued to expand with the forward motion, and the concentration of abrasives with material removal ability in the outer zone became relatively less. According to the previous discussion, although the total amount of abrasives arriving at the target unit area in unit time was large, the total number of abrasives with effective material removal power was reduced compared to that at the top and middle sections of the hole. Therefore, the diameter of drilled holes became small, resulting in D_{ex} being often smaller than D_m and D_{en}.

Some broken abrasives bouncing back from the blind-hole bottom still had strong material removal power because of large stagnation pressure [37, 38]. It is another reason resulting in a large D_m. As evaluated previously, D_{en} increased with *SOD* and *AMFR*, indicating that the first reason discussed above might be the main cause leading to a large D_m. However, it needs more experimental evidence for confirmation.

D of each hole was calculated with Eq. (1), whose bar graphs are illustrated in Fig. 5a. The required diameter of drilled holes is O_b = 6.000 mm. As seen in Table 2, D_{en}, D_m, and D_{ex} increase with each of *SOD*, *WJP*, and *AMFR*, resulting in *D* much larger than O_b. Based on these, the largest *D* naturally appears at the largest *SOD*, *WJP*, and *AMFR*. According to Table 2, the mean *D* of all 27 holes is nearly 6.151 mm.

Using the results listed in Table 2, single-objective optimization determines that the largest *S/N* ratios of *D* are located at levels = 1, 1, and 1 for *SOD*, *WJP*, and *AMFR*, respectively, corresponding to *SOD* = 1 mm, *WJP* = 1600 bar, and *AMFR* = 200 g/min, at which *D* was measured as 6.077 mm, showing that the optimal *D* appears at the smallest *SOD*, *WJP*, and *AMFR*, agreeing with the conclusion obtained previously. Employing Eq. (6), the optimal *D* is predicted as approximately 6.078 mm, deviating from the measured *D* at the optimum levels by only 0.001 mm.

Table 4 gives the ANOVA results of eight hole-quality parameters, *D*, ΔD, K_f, C_{yl}, R_e, P_{erp}, R_a, and R_z. The contributions to *D* from *AMFR*, *SOD*, and *WJP* are 45.86%, 29.18%, and 20.47%, respectively, indicating that *AMFR* has the greatest influence on *D*, followed by *SOD* and *WJP*. In addition, the total contribution from the quadratic product terms is no more than 2.94%, indicating that their effect on *D* can be negligible. For *D*, each linear factor has statistical significance, while each quadratic product term is not statistically significant. The error of contribution to *D* from other sources not included in Table 4 is only 1.55%, showing that other sources can be negligible.

ΔD is a more important parameter than *D* when evaluating the quality of holes. The reason is that ΔD is the reflection of the uniform consistency of *D*, while *D* can be easily adjusted to the required value by changing *CMD*. Figure 5b illustrates that the largest ΔD is 0.098 mm, corresponding to the 11th hole. Based on Table 2, the mean ΔD of all holes is only 0.022 mm, which is not large. A small average ΔD indicates that ΔD is easy to satisfy the requirement under the current drilling condition.

As per Table 2, the largest *S/N* ratios of ΔD are determined to be at levels = 1, 2, and 3 for *SOD*, *WJP*, and *AMFR*, respectively, at which ΔD was measured as 0.017 mm. Using Eq. (6), the optimal ΔD is predicted as nearly 0.009 mm. No ΔD value of the same hole is currently available in the literature about AWJD of various aluminium alloys [29–32]. Naturally, a comparison with previous experimental results cannot be performed.

Table 5 lists the parameters used to calculate *CI* of the predicted ΔD, P_{erp}, and K_f. Three of the parameters (T_{dof}, V_2, and V_e) were calculated by AVONA. In combination with Eq. (8), *CI* of the predicted ΔD was computed as $\pm$ 0.023 mm. The range of predicted values covered the measured ΔD.

As tabulated in Table 4, the contributions to ΔD from the linear model and 2-way interactions are 22.10% and 49.83%, respectively, suggesting that the influence of the linear model on ΔD is smaller than that of 2-way interactions. *WJP* is the most important factor affecting ΔD for the linear model. All *P*-values are considerably higher than 0.05 for ΔD, indicating that all variables collected in Table 4 are statistically insignificant. In addition, the error of the contribution from other sources not listed in Table 4 amounts to 28.07%, illustrating that other sources not listed herein have a the great influence on ΔD.

K_f reflects the relationship between *H* and the difference in D_{en} and D_{ex}. For a given material thickness, K_f is determined only by the difference in D_{en} and D_{ex}. The variation rule illustrated in Fig. 5c is not the same as that in Fig. 5b.

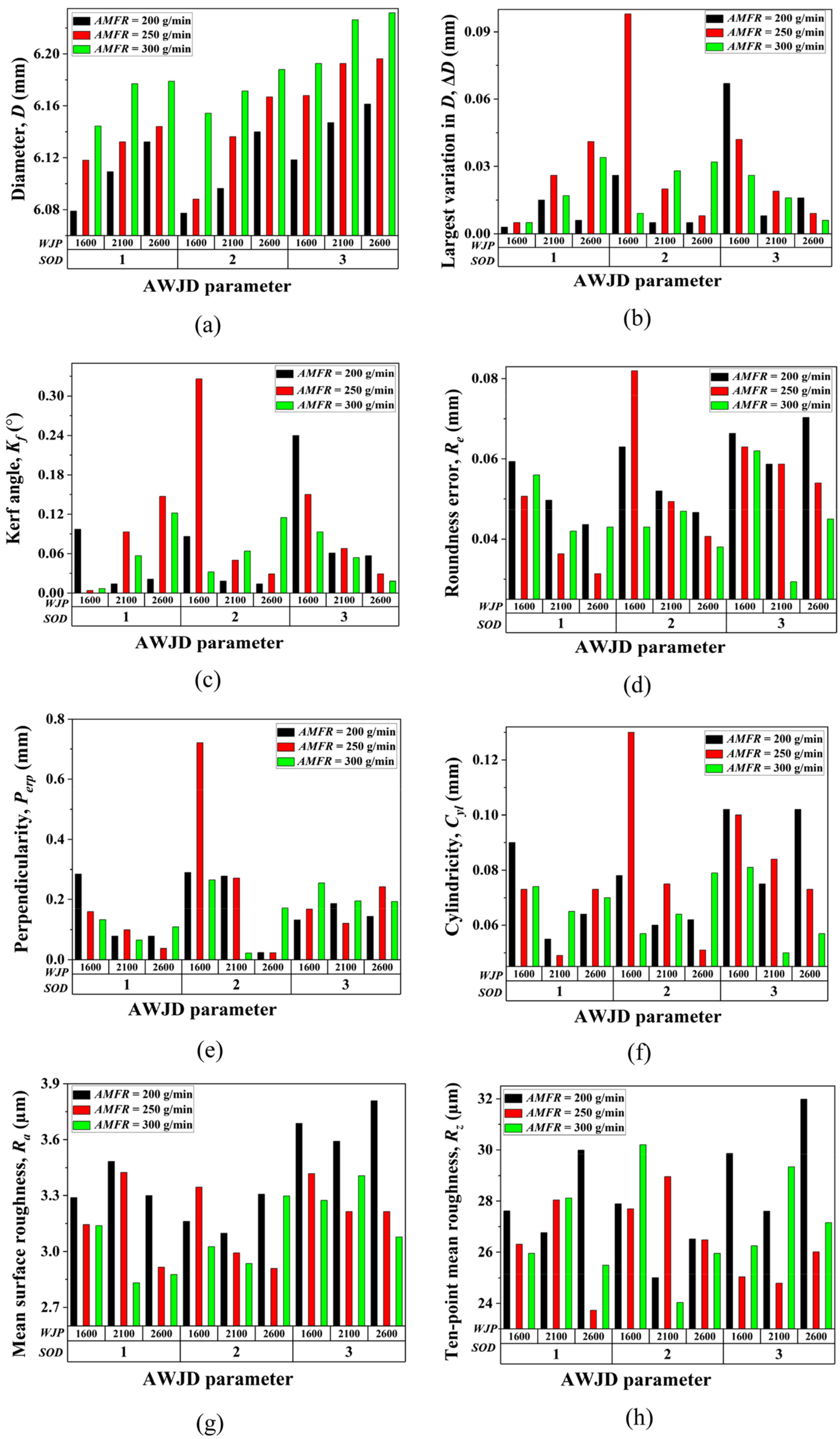

Fig. 5 Bar graphs of (**a**) D, (**b**) ΔD, (**c**) K_f, (**d**) R_e, (**e**) P_{erp}, (**f**) C_{yl}, (**g**) R_a and (**h**) R_z versus each AWJD parameter

Table 4 ANOVA results for D, ΔD, K_f, C_{yl}, R_e, P_{erp}, R_a, and R_z

Source	D		ΔD		K_f		C_{yl}	
	Contrib	*P*-value	Contrib	*P*-value	Contrib	*P*-value	Contrib	*P*-value
Model	98.45%	0.000	71.93%	0.447	82.67%	0.140	71.75%	0.453
Linear	95.51%	0.000	22.10%	0.461	57.93%	0.028	41.89%	0.183
SOD	29.18%	0.000	1.72%	0.788	25.09%	0.028	14.10%	0.198
WJP	20.47%	0.000	14.90%	0.182	12.92%	0.108	23.56%	0.088
AMFR	45.86%	0.000	5.47%	0.490	19.92%	0.047	4.23%	0.572
2-way interactions	2.94%	0.378	49.83%	0.417	24.74%	0.547	29.86%	0.718
SOD×*WJP*	1.33%	0.239	22.86%	0.258	11.16%	0.351	3.64%	0.897
SOD×*AMFR*	0.85%	0.418	11.28%	0.556	5.34%	0.663	11.00%	0.569
WJP×*AMFR*	0.76%	0.468	15.69%	0.412	8.24%	0.483	15.22%	0.428
Error	1.55%		28.07%		17.33%		28.25%	
Total	100.00%		100.00%		100.00%		100.00%	
Source	R_e		P_{erp}		R_a		R_z	
	Contrib	*P*-value	Contrib	*P*-value	Contrib	*P*-value	Contrib	*P*-value
Model	91.39%	0.015	78.38%	0.250	93.09%	0.007	88.51%	0.040
Linear	40.14%	0.011	40.23%	0.117	51.48%	0.002	24.54%	0.087
SOD	17.48%	0.012	11.23%	0.188	12.96%	0.015	0.09%	0.970
WJP	13.88%	0.023	25.13%	0.046	4.76%	0.123	5.88%	0.192
AMFR	9.28%	0.054	3.87%	0.517	33.77%	0.001	18.48%	0.022
2-way interactions	51.25%	0.029	38.15%	0.421	41.61%	0.028	64.06%	0.036
SOD×*WJP*	13.81%	0.075	19.43%	0.223	13.14%	0.051	22.39%	0.048
SOD×*AMFR*	15.39%	0.059	7.96%	0.593	11.32%	0.072	23.21%	0.044
WJP×*AMFR*	22.05%	0.025	10.76%	0.463	17.15%	0.026	18.47%	0.075
Error	8.61%		21.62%		6.91%		11.49%	
Total	100.00%		100.00%		100.00%		100.00%	

Table 5 Parameter to calculate *CI* of ΔD, P_{erp}, and K_f

Parameter	ΔD	P_{erp}	K_f	Parameter	ΔD	P_{erp}	K_f
T_{exp}	27	27	27	V_2	20	20	20
T_{dof}	6	6	6	V_e	0.000099	0.01555	0.006208
α	0.05	0.05	0.05	n_{eff}	3.8571	3.8571	3.8571
r	1	1	1	$F_{\alpha, 1, V2}$	4.35	4.35	5.35

It can be explained by the fact that ΔD used in Fig. 5b is the largest change in D, while ΔD used in Eq. (3) is the difference only between the entrance and exit. Figure 5c illustrates that K_f has a complicated relationship with *SOD*, *WJP*, and *AMFR*. Even if two variables remain invariable, K_f has almost no obvious relationship with the remaining one. Based on Table 2, the average K_f of all 27 holes is 0.077°, which is very small. From Fig. 5c, it can be observed that the poorest K_f is 0.326°, corresponding to *SOD* = 2 mm, *WJP* = 1600 bar, and *AMFR* = 250 g/min. At the same time, Fig. 5c shows that only a few holes have K_f larger than 0.100°. To the authors' knowledge, no K_f values have been reported to date for AWJD of various aluminium alloys with AWJ.

Only Ralph et al. [10] and Elajrami et al. [19] measured K_f when drilling aluminium alloys employing MD approach. The mean values of K_f reported in [10] are collected in Table 6. Their results are much poorer than the present one with or without pilot holes. Elajrami et al. [19] measured K_f and found that it was greatly reduced by pilot holes, but no accurate K_f results were reported. Ravi and Srinivasu [32] reported that the minimum value of K_f measured in their experiment was 0.114°, significantly larger than the present one.

Using the data given in Table 2, the largest *S*/*N* ratios of K_f are determined to be at levels = 1, 2, and 3 for *SOD*, *WJP*, and *AMFR*, respectively, which are the same as those of ΔD. K_f was measured as 0.057° under the optimal condition. Using Eq. (6), the optimal K_f is predicted as 0.025°. Using the results in Table 5, *CI* of the predicted K_f was computed as nearly ± 0.184°. The range of predicted values covered the experimental K_f of 0.057°.

Table 6 Comparison of K_f, R_e, R_{en}, R_{ex}, and C_{yl} reported in the open literature with those measured in the current work

Source	K_f (°)	R_e (mm)	R_{en} (mm)	R_{ex} (mm)	C_{yl} (mm)
MD method	3.925° without pilot holes [10]; 0.700° with pilot holes [10];	0.020 – 0.055 [24] <0.1 [17]; <0.03 [23]	0.00692 – 0.00274 [9]	0.0041 – 0.00338 [9]	0.025 – 0.095 [24]
AWJ method	≥0.114° [32]		≥0.0515 [32]	≥0.1394 [32]	>0.3 [31] ≥0.089 [32]
This work	≤0.326°	≤0.082	≤0.130	≤0.102	≤0.130

Based on Table 4, the contributions to K_f from *SOD*, *WJP*, and *AMFR* are 25.09%, 12.92%, and 19.92%, respectively, showing that *SOD* has the most effect on K_f, followed by *AMFR* and *WJP*. Furthermore, only *AMFR* and *SOD* have a *P*-value smaller than 0.05, indicating that only the two linear factors have statistical significance. In addition, all quadratic product terms have *P*-values greatly larger than 0.05, predicting that they are all statistically insignificant. Different from that of *D*, for K_f, the error from another source not listed in Table 4 reaches 17.33%, showing that other variables ignored in the current model also have some influence on K_f, while they were not considered in this model.

3.2 Effect of AWJD parameters on R_e, P_{erp}, and C_{yl}

As shown in Table 3, R_{em} is almost the poorest at $SOD = 1$ mm. R_{ex} is relatively poor among the three values of the same hole. All R_{em}, all R_{en} except for the 11th hole, and all R_{ex} except for the 19th, 20th, and 25th holes are smaller than 0.100 mm, illustrating that almost all R_{en}, R_{em}, and R_{ex} are encouraging except for only a few holes. R_e of the holes in this work is good except for the 11th, 19th, 20th, and 25th holes, for which R_{en} or R_{ex} is no less than 0.100 mm. Since R_e of one hole is determined by the difference in *D* between the minimum circumscribed circle and maximum inner circle as well as R_e is determined by R_{en}, R_{em}, and R_{ex}, it is not difficult to understand why the four holes (11th, 19th, 20th, and 25th) have poor R_e.

Figure 5d displays that the smallest and largest values of R_e are 0.029 and 0.082 mm, corresponding to the 24th and 11th holes, respectively. As per Table 3, the average R_e of all 27 holes is nearly 0.051 mm, which is larger than that of holes drilled through Al2024 aluminium alloy using twist drill bits [24], as seen in Table 6. Giasin et al.[9]. employed carbide twist drills to drill Al2024-T3 aluminium alloy and measured R_{en} and R_{ex}. Kurt et al. [17] reported that the R_e was smaller than 0.1 mm for all holes when they used HSS drills to machine Al2024 aluminium alloy. Abdelhafeez et al. [23] reported that the R_e of all holes was smaller than 30 µm when they used carbide drills to cut Al2024 aluminium alloy. Ravi and Srinivasu [32] found that the minimum values of R_{en} and R_{ex} were 0.0515 and 0.1394 mm when drilling Al6061 aluminium alloy, respectively. As a result, R_e in [9, 17, 23, 24] is overall superior to those measured in this work, showing that the present AWJD parameters should be further optimized although R_{en} and R_{ex} measured in this work are significantly superior to those reported in [32].

Similar to D_{en}, D_m, and D_{ex}, single-objective optimization was not done for R_{en}, R_{em}, and R_{ex}. Using the data presented in Table 2, the largest *S*/*N* ratios of R_e are calculated to be at $SOD = 1$ mm, $WJP = 2600$ bar, and $AMFR = 200$ g/min, at which R_e was measured as 0.044 mm. Equation (6) predicted that the optimal R_e was 0.034 mm. The deviation between them is only 0.010 mm. The optimal predictive R_e was slightly larger than those reported in [9, 23] and close to those available in [24]. No matter what the value of *TS* was, the minimum R_e measured by Tekaüt was greater than 0.2 mm whether for R_e, R_{ex}, or R_{en} when using AWJ to drill Al7075 aluminium alloy [31]. The quality of their Re was much poorer than that reported in this work. The reason might be that the AWJD parameters used in the current work were the results of screening by drilling trials, which might not be in [31].

According to Table 4, the percentage contributions to R_e from *SOD*, *WJP*, and *AMFR* are 17.48%, 13.88%, and 9.28%, respectively, indicating that *SOD* has the most important effect on R_e among the three linear factors. The total contributions from the linear model and 2-way interactions are 40.14% and 51.25%, respectively, showing that the effect of 2-way interactions on R_e is more important than the linear model. As observed in Table 4, only *SOD*, *WJP*, and $WJP \times AMFR$ have *P*-values smaller than 0.05, indicating that only these three terms are statistically significant for R_e. As listed in Table 4, the contribution to R_e from other sources not listed is only 8.61%, showing that other variables neglected herein have little effect on R_e.

As can be observed in Table 3 and Fig. 5e, P_{erp} varies from 0.022 to 0.721 mm and the smallest P_{erp} corresponds to the 15th hole, which was drilled with $SOD = 2$ mm, $WJP = 2100$ bar, and $AMFR = 300$ g/min; and the largest P_{erp} corresponds to the 11th hole, which was drilled with $SOD = 2$ mm, $WJP = 1600$ bar, and $AMFR = 250$ g/min. Figure 5e clearly shows that P_{erp} values of most holes are larger than 0.100 mm. According to Table 3, the mean P_{erp}

of all holes is approximately 0.176 mm, which is larger than that of holes drilled through Al2024 aluminium alloy using twist drills [24]. However, no P_{erp} of holes drilled through aluminium alloy with AWJ has been reported to this day. P_{erp} measured herein is somewhat large compared to those reported in [24]. As discussed in [10, 19], some hole-quality parameters such as K_f, P_{erp}, and C_{yl} could be improved by pilot holes.

Based on the data collected in Table 3, the largest *S*/*N* ratios of P_{erp} are determined to be at levels = 1, 3, and 3 for *SOD*, *WJP*, and *AMFR*, respectively, corresponding to the 9th hole. As listed in Table 3, P_{erp} of the 9th hole is 0.109 mm. Equation (6) predicted that the optimal P_{erp} was nearly 0.034 mm. Using the results listed in Table 5, *CI* of the predicted P_{erp} was determined to be ± 0.292 mm. Therefore, the range of the predicted P_{erp} covered the measured one at the optimum levels although the difference between them looked a bit big.

As listed in Table 4, the contribution to P_{erp} from all linear factors reaches 40.23%, while that from all quadratic product terms is 38.15%, suggesting that the contribution to P_{erp} from the three linear factors is equivalent to that from three quadratic product terms. According to Table 4, the *P*-value of only *WJP* is smaller than 0.05, indicating that only it is statistically significant. Similar to R_e, K_f, and ΔD, the contribution to P_{erp} from another source is large, indicating that another source not considered in the current model has an important effect on P_{erp}, too.

Cylindricity is the degree to which a hole deviates from the ideal inscribed cylinder. The smaller the deviation, the better the cylindricity will be. Carefully examining the bar graphs shown in Fig. 5f, it can be immediately found that the lowest C_{yl} is located the 5th hole, which was drilled using *SOD* = 1 mm, *WJP* = 2600 bar, and *AMFR* = 250 g/min. Table 3 shows that the smallest C_{yl} is 0.049 mm. The highest C_{yl} is located the 11th hole, which was drilled with *SOD* = 2 mm, *WJP* = 1600 bar, and *AMFR* = 250 g/min. Table 3 shows the largest C_{yl} is 0.130 mm. Based on Table 3, the mean value of C_{yl} is calculated as 0.077 mm.

Only Tekaüt [31] measured C_{yl} and evaluated the effect of *TS* on C_{yl} of holes drilled through Al2024 aluminium alloy using AWJ. The smallest C_{yl} was 0.3 mm [31], which was greatly larger than the maximum reported in the present work. Only Aamir et al.[24]. measured C_{yl} and evaluated the effect of spindle speed and feed rate on C_{yl} of holes drilled through Al2024 aluminium alloy employing twist drills. Their C_{yl} was 25 to 95 μm [24], which was slightly superior to the present results. Ravi and Srinivasu [32] reported that the minimum value of C_{yl} was 89.3 μm, which was greatly poorer than the present one.

Based on Table 3, Single-objective optimisation obtains that the optimal C_{yl} is at levels = 1, 2, and 3, corresponding to *SOD* = 1 mm, *WJP* = 2100 bar, and *AMFR* = 300 g/min, respectively, at which C_{yl} was measured as 0.065 mm. Equation (6) predicted that the optimum C_{yl} was 0.045 mm. The difference between the predicted and measured C_{yl} is 0.020 mm, which is small.

Based on Table 4, the percentage contributions to C_{yl} from *SOD*, *WJP*, and *AMFR* are 14.10%, 23.56%, and 4.23%, respectively, indicating that *WJP* has the most important effect on C_{yl}, followed by *SOD*, among the three linear factors. The largest contribution to C_{yl} is from *WJP* × *AMFR*, followed by *SOD* × *AMFR*, among the 2-way interactions. As seen in Table 4, all factors of C_{yl} have *P*-values larger than 0.05, indicating that none of them was statistically significant for C_{yl}.

3.3 Effect of AWJD parameters on R_a and R_z

Figure 5g in combination with Table 3 shows that the highest and lowest values of R_a are 3.808 and 2.832 μm, corresponding to the 25th and 6th holes, respectively. Figure 5h in combination with Table 3 illustrates that the largest and smallest values of R_z are 31.987 and 23.727 μm, located at the 25th and 8th holes, respectively. Based on Table 3, the mean values of R_a and R_z are 3.228 and 27.139 μm, respectively, which are slightly larger than the requirements by SANDVIK tool manufacturer [4]. Carefully examining R_a and R_z in Figs. 5g and 5h, almost no clear change rule can be found.

Using the data listed in Table 3, the largest *S*/*N* ratios of R_a are determined to be at levels = 2, 2, and 3, corresponding to *SOD* = 2 mm, *WJP* = 2100 bar, and *AMFR* = 300 g/min, respectively; and the largest *S*/*N* ratios of R_z are located at levels = 1, 2, and 2, which correspond to *SOD* = 1 mm, *WJP* = 2100 bar, and *AMFR* = 250 g/min, respectively. Equation (6) predicted that the optimal R_a and R_z as 2.978 and 25.911 μm, respectively. Drilling holes with the optimal parameters, R_a was measured as 2.935 μm, deviating from the predictive one by only 1.47%; and R_z was measured as 28.044 μm, deviating from the predicted one by 7.59%.

Only Lathif et al. [30] used *AMFR*, *WJP*, *SOD*, and *TS* as AWJD parameters to cut 29 holes through Al7075 aluminium alloy and measured R_a. The R_a range and average R_a in [30] is collected in Table 7. As seen in Table 7, R_a values measured in this work are distributed in a narrow range compared to those in [30] and the average R_a available in [30] was slightly larger than that reported in this work. The optimal R_a in [30] was 1.494 μm, located at *SOD* = 1.99 mm, *WJP* = 3403.3 bar, *TS* = 311.36 mm/min, and *AMFR* = 477.31 g/min [30]. However, using their optimal processing parameters to drill holes in the current work, the visual inspection showed that R_{ex} was very poor. No experimental R_z results are currently available in the open literature using AWJD.

Table 7 Comparison of R_a and R_z reported in the open literature with those measured in this work

Source	Average R_a (μm)	R_a (μm)	R_z (μm)
MD method		1.159 – 7.96 [9], 0.6 – 3.6 [15], 3.0 – 8.0 [17], 5.91 – 7.9 [18], 6.118 – 8.114 [20]	unavailable
AWJD method	3.988 [30]	1.53 – 6.1 [30]	unavailable
This work	3.228	3.808 – 2.832	31.987 – 23.727

Several experimental groups drilled holes through Al2024 aluminium alloys using twist drills and measured R_a [9, 15, 17–20]. The values of R_a were summarised in Table 7. A comparison illustrates that only some results of R_a in [9, 15] are superior to the current ones. Note that Ralph et al. [10] and Elajrami et al. [19] employed pilot holes to improve the quality of holes drilled with MD approaches. The conclusion was that R_a could be significantly reduced. As further investigations, our experimental group will soon employ pilot holes to improve the quality of holes drilled through Al2024-T3 aluminium alloy with AWJ.

As seen in Table 4, the percentage contributions to R_a from the linear model and 2-way interactions are 51.48% and 41.61%, respectively, showing that they have almost the same influence on R_a. Of the three linear factors, *AMFR* had the greatest effect on R_a, followed by *SOD*. Of all quadratic product terms, *WJP* × *AMFR* had the greatest influence on R_a. In addition, for R_a, *P*-values of *SOD*, *AMFR*, and *WJP* × *AMFR* are less than 0.05, showing that only these three terms have statistical significance.

However, the contribution to R_z from the quadratic product terms amounts to 64.06%, while that from the linear factors is only 24.54%, showing that the influence of quadratic product terms on R_z is more important than that of the linear factors. For R_z, only *AMFR*, *SOD* × *WJP*, and *SOD* × *AMFR* are statistically significant. The errors of contribution from the sources not listed in Table 4 are only 6.91% and 11.49% for R_a and R_z, respectively, indicating that the effect of other sources not considered on R_a and R_z is not important.

Finally in this section, for convenience of comparison, Table 8 summarises the mean value, optimal AWJD parameters obtained by single-objective optimisation, and measured and predicted values of each hole-quality parameter at the optimal levels.

3.4 SEM analysis of machined surface of holes

To show a full hole-quality image, Figs. 6a – 6c give SEM pictures of the machined surface of the same hole at its top, middle, and bottom sections, which were taken by SEM with nearly 40 × magnification. The hole used in Fig. 6 was drilled at *SOD* = 1 mm, *WJP* = 2100 bar, and *AMFR* = 250 g/min.

As seen in Fig. 6, the machined hole-wall surfaces are smooth at low magnification. Certain surface chips and craters can be observed, especially in Fig. 6(c), showing that machined surface at the hole top is highly smooth compared to that at the bottom section. No embedded abrasives can be found in Fig. 6. No obvious burrs, damages or surface cracks can be observed. Hole-wall surfaces of many holes were inspected by SEM at the various levels of sub-millimetre scale. A similar conclusion is obtained for each hole.

Figure 7a shows the local surface image of the hole drilled at *SOD* = 1 mm, *AMFR* = 200 mm/min, and *WJP* = 2100 bar, which was taken by SEM with 13.2 k × magnification. Note that certain local surface was rather smooth even at such high magnification. In this figure, surface chips are clearly seen; traits from abrasive plough are distinctly illustrated;

Table 8 Summary of the eight hole-quality parameters

Hole-quality parameter	Average value	Optimal drilling parameters			Optimal expt	Predicted value
		WJP (bar)	*AMFR* (g/min)	*SOD* (mm)		
D (mm)	6.151	1600	200	1	6.077	6.078
Δ*D* (mm)	0.022	2100	300	1	0.017	0.009
K_f (°)	0.077	2100	300	1	0.025	0.057
R_e (mm)	0.051	2600	200	1	0.044	0.034
P_{erp} (mm)	0.176	2600	300	1	0.109	0.034
C_{yl} (mm)	0.077	2100	300	1	0.065	0.045
R_a (μm)	3.228	2100	300	2	2.935	2.978
R_z (μm)	27.139	2100	250	1	28.044	25.911

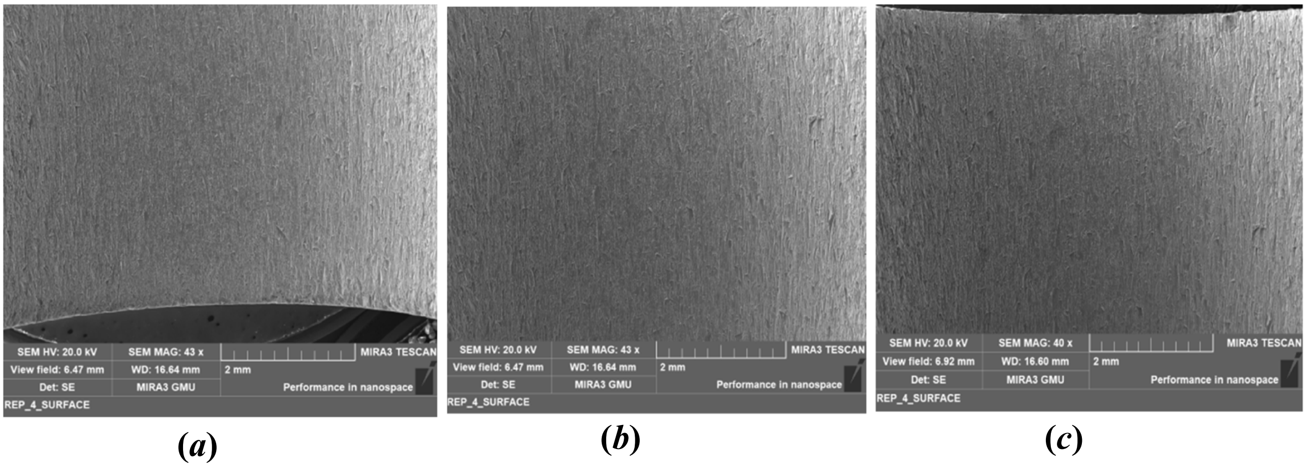

Fig. 6 SEM pictures of the hole drilled through Al2024-T3 aluminium alloy at (**a**) hole top, (**b**) middle, and (**c**) bottom of at low magnification

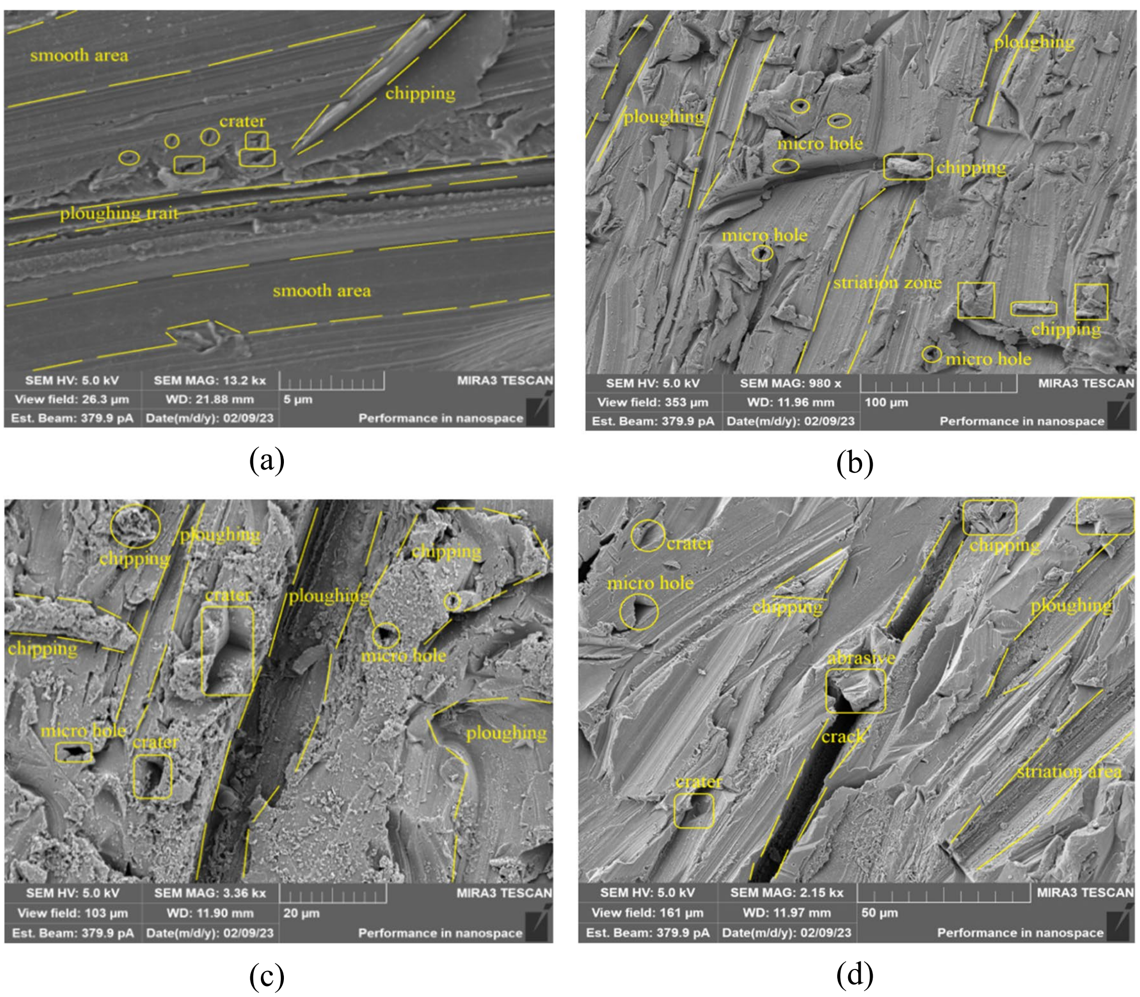

Fig. 7 SEM pictures about smooth zone, surface chipping, ploughing trait, crater, striation zone, micro-hole, and crack

and craters and micro holes generated from abrasive impingement are expressly shown. The situations described in Fig. 7a can be observed at many places of each hole. Surface roughness was generated due to these micro holes, craters, surface chips, and ploughing traits [39].

Figure 7b illustrates several ploughing marks and long grooves generated by abrasive plough and micro holes originated from abrasive hits due to the turbulence of AWJ, taken by SEM with 980 × magnification. The hole used for Fig. 7b was drilled at $SOD = 3$ mm, $WJP = 1600$ bar, and $AMFR = 250$ mm/min. It should be noted that the magnification of picture illustrated in Fig. 7a is more than 13 times that in Fig. 7b, further proving that the surface in Fig. 7a was rather smooth compared to Fig. 7b and that surface chips in Fig. 7b should be much larger than those in Fig. 7a. Ploughing marks and long grooves shown in Fig. 7b were also seen by Ravi and Srinivasu [32] when they drilled Al6061 aluminium alloy using AWJ.

Striation zone was generated by a series of ridges which were produced by ploughing action of abrasives, as shown in Fig. 7b. Craters and micro holes were generated from abrasive strikes on wall surface due to the turbulence of AWJ [37, 38], while ploughing marks were produced by abrasives with high kinetic energy when machining hole-wall surface. Both ploughing action and strike on the hole-wall surface by abrasive particles could form the surface chips. Ploughing action usually generated a narrow and aligned mark along the direction of AWJ transmission [38], as illustrated in Fig. 7b. Abrasive ploughing action was one of the main processes of material removal from Al2024-T3 aluminium alloy. A continuous ploughing action caused a smooth zone illustrated in Figs. 7a and 7b.

Figures 7c and 7d demonstrate more surface chips, abrasive ploughing traits, craters, and micro holes, which were taken for holes drilled with $SOD = 2$ mm, $WJP = 1600$ bar, and $AMFR = 200$ g/min as well as $SOD = 2$ mm, $WJP = 2100$ bar, and $AMFR = 300$ g/min, respectively. EDX spectroscopy confirmed that the embedded abrasive particle in Fig. 7d was an abrasive. It should be that Ravi and Srinivasu [32] also observed numerous surface chips, ridges, craters, and micro holes with various dimensions when they employed AWJ to drill Al6061 aluminium alloy. In addition, Fig. 7d shows a crack. As seen in Fig. 7d, the width of the crack was greatly smaller than the dimension of abrasive embedded into the hole-wall surface. Hence, the crack should be generated by abrasive impingement on the surface, not by an abrasive plough. The abrasive entering the crack was embedded by impinging.

Figure 8a presents the hole-surface image taken by SEM at the sub-micron scale. In Fig. 8a, one can find an abrasive particle embedded into the surface at the sub-micron scale. The hole employed for Fig. 8a was drilled at $SOD = 1$ mm, $WJP = 1600$ bar, and $AMFR = 200$ g/min. To confirm that the abrasive particle shown in Fig. 8a was indeed an abrasive, Fig. 8e gives its EDM spectroscopy. By comparison of spectroscopy in Fig. 8e with that in Figs. 3b and 3c, one can instantly conclude that the abrasive particle shown in Fig. 8a is an abrasive. From the ploughing marks shown in Fig. 8a, one could clearly see the drilling direction of AWJ. Compared to Fig. 7, Fig. 8a shows more surface chips. Similar to Fig. 7, these surface chips consisted of peaks of surface roughness; while ploughing traits, craters, and micro holes were composed of valleys [39].

Figures 8b and 8c show pictures of embedded abrasives, smooth zones, surface chips, and abrasive ploughing marks taken by SEM at high magnification. The hole employed in Figs. 8b and 8c was the same one, drilled at $SOD = 1$ mm, $WJP = 2600$ bar, and $AMFR = 200$ g/min. EDX spectroscopy clearly confirms that the embedded abrasive particles in Fig. 8b and Fig. 8c are abrasives. Then embedded abrasives were also observed by Ravi and Srinivasu in their experiment [32]. From these ploughing traits, one can clearly observe the drilling direction of AWJ, as marked by the arrow in Figs. 8b and 8c. Similar to Fig. 7, smooth zones can be clearly seen in Figs. 8b and 8c at such a high resolution.

Surface microstructures illustrated in Figs. 7 and 8 were almost seen for each hole, showing almost the same mechanisms of material removal from Al2024-T3 aluminium alloy under various AWJD conditions used in the current work.

Various furrows ploughed by abrasives as well as various craters, micro holes, and cracks generated by abrasive impingement formed various valleys. And surface chips and ridges originating from abrasive plough formed various peaks, as discussed above. These valleys and peaks formed the surface roughness. It is worth noting that the distributions of these valleys and peaks were in irregular patterns [39], which explain why no variation rules of R_a and R_z with AWJD parameters are observed in Sect. 3.3. Figure 8d illustrates the image of a broken abrasive embedded into the surface of the hole, taken by SEM at 1.21 k × magnification. The hole used in Fig. 8d was drilled at $SOD = 1$ mm, $AMFR = 300$ g/min, and $WJP = 1600$ bar. Figure 8e shows EDX spectroscopy of the broken abrasive particle. According to EDX spectrum shown in Fig. 8e, it is concluded that the broken particle is indeed an abrasive particle since it is smaller than nominal abrasive size.

Figure 8d illustrates many ploughing traits of abrasives. According to these traits, one could accurately determine the drilling direction of AWJ, as shown by the arrow in Fig. 8d. Numerous surface chips in Fig. 8d were generated by abrasives, similar to Figs. 7 and 8. When a broken abrasives returned from the bottom of a blind hole, it might possess high kinetic energy and could remove materials from the wall surface. These abrasive particles were embedded into the surface because of the turbulence of AWJ generated by the counter- action between the forward-moving waterjet

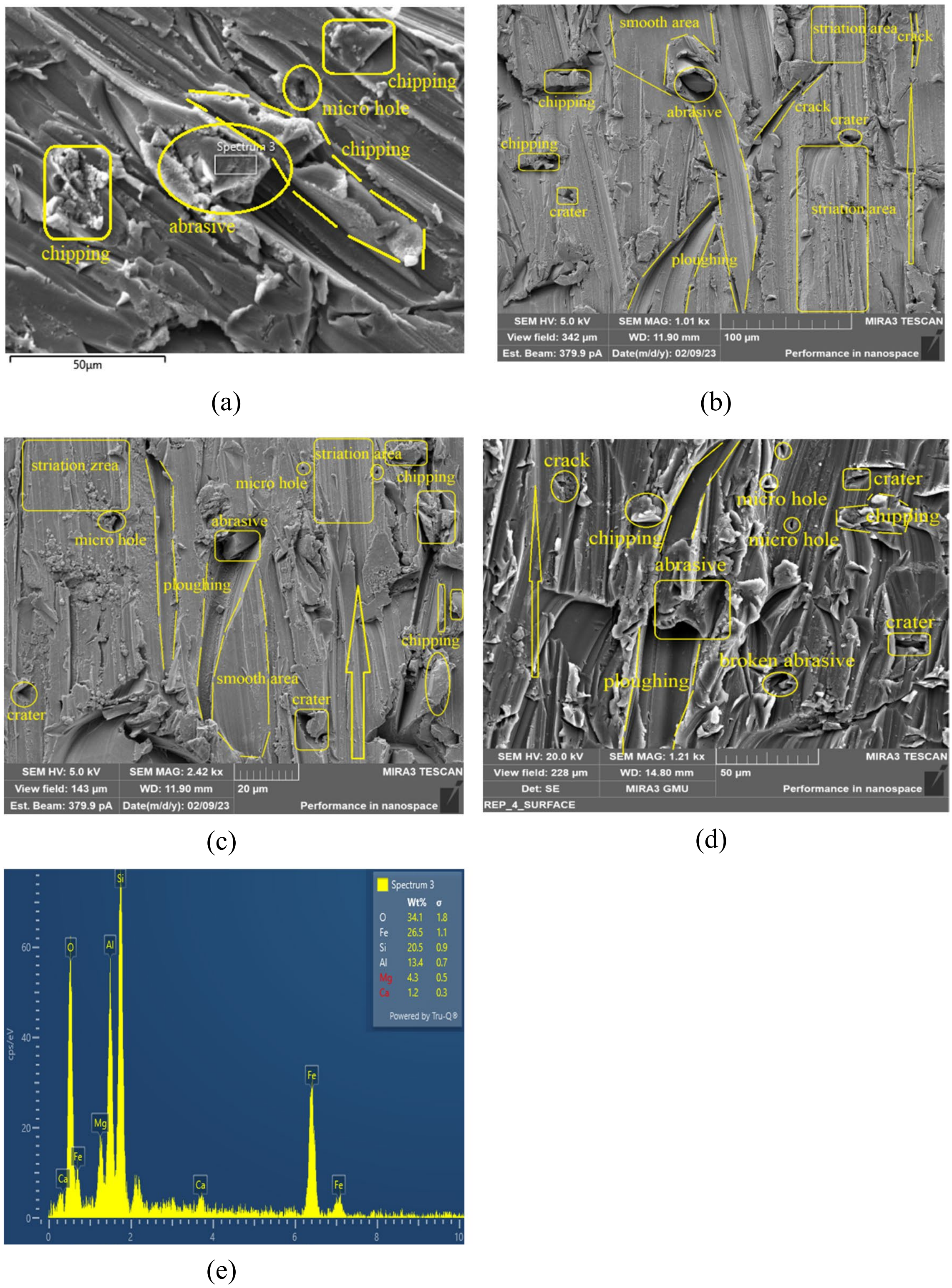

Fig. 8 (**a**) Surface microstructure containing embedded abrasives at 1.81 k×, (**b**) 1.01 k×, (**c**) 2.42 k×magnification, (**d**) 1.21 k×, and (**e**) their EDX spectroscopy

and returning waterjet [37, 38]. Hence, secondary removal of abrasives was also one of the material removal mechanisms. The embedded abrasives and broken abrasives were found most commonly in the middle section of a hole. It is the turbulence that made the abrasives deflect the forward direction of AWJ and impact the surface, forming craters and micro holes shown previously in Fig. 7 and in Fig. 8, which also made the abrasives embedded in the crack shown previously in Fig. 7d.

3.5 Multi-objective optimization

D, ΔD, K_f, R_e, C_{yl}, P_{erp}, R_a, and R_z, were employed for multi-objective optimization [35, 37]. Through a series of calculations, the values of GRG of each hole were obtained, as presented in Table 3. Table 3 also gives the order of the GRG from smallest to largest. Note that ω_p of each hole-quality parameter was equal when calculating the GRG. As per the GRG ranking, the 17th hole has the optimal quality, for which the optimum *SOD*, *WJP*, and *AMFR* are 2 mm, 2600 bar, and 250 g/min, respectively; and the optimal hole-quality parameters are $D = 6.167$ mm, $\Delta D = 0.008$ mm, $K_f = 0.029°$, $C_{yl} = 0.051$ mm, $P_{erp} = 0.033$ mm, $R_e = 0.041$ mm, $R_a = 2.909$ µm, and $R_z = 26.480$ µm.

3.6 Adjustment of CMD

The above hole-quality parameters determined by multi-objective optimization were measured for holes drilled at $CMD = 6.000$ mm. As discussed previously, D was always larger than the nominal value when using AWJ to drill Al2024-T3 aluminium alloy. To make D close to 6.000 mm required in this work, *CMD* was adjusted to 5.900, 5.800, and 5.700 mm to perform the confirmative drilling trials to reduce D at the optimal levels. Three holes were drilled at each *CMD* using the optimal AWJD parameters at $TS = 10$ mm/min. Table 9 collects these results and their comparison with the ideal values.

As observed in Table 9, the differences between the D, ΔD, R_e, P_{erp} and the ideal values when $CMD = 5.800$ mm are smaller than 0.050 mm, indicating that the quality of these four parameters is very good. Both K_f and R_e are very small, similar to the results obtained at $CMD = 6.000$ mm. R_a and R_z measured at $CMD = 5.800$ mm are very close to those obtained at $CMD = 6.000$ mm. The comparison shows that adjustment of *CMD* is an appropriate approach to make D close to 6.000 mm. As a conclusion, drilling holes at the optimal levels with an appropriate *CMD* can make D close to the nominal diameter without reducing the quality of other hole-quality parameters.

As a conclusion, the quality of the holes drilled at the optimal levels of *SOD*, *WJP*, and *AMFR* when $CMD = 5.800$ mm is encouraging compared to that reported previously.

4 Conclusions

In this work, three variable AWJD parameters, $WJP = 1600$, 2100, and 2600 bar, $SOD = 1$, 2, and 3 mm, and $AMFR = 200$, 250, and 300 g/min, were used to drill Al2024-T3 aluminium alloy for keeping $TS = 10$ mm/min. A full factorial experimental design was used to plan the holes being drilled. Eight hole-quality parameters, namely D, ΔD, K, C_{yl}, P, R_e, R_a, and R_z, were measured and compared to the available measurements. Single- and multi-objective optimization was performed. The effect of *SOD*, *AMFR*, and *WJP* on these parameters was evaluated. Summarizing the results in the present work, three main conclusions are obtained.

(1) R_e was significantly affected by *TS*. Generally, the greater the *TS*, the poorer the R_{ex} would be. Visual inspection confirmed that R_{ex} was very poor when $TS \geq 50$ mm/min. The edge surface finish of holes was visually satisfactory for $TS \leq 30$ mm/min when $SOD = 2$ mm, $WJP = 2100$ bar, and $AMFR = 200$ g/min.

Table 9 Measured data at the optimal levels ($SOD = 2$ mm, $AMFR = 250$ g/min, and $WJP = 2600$ bar) and different values of *CMD* as well as comparison with the ideal values

Type	*CMD* (mm)	D (bar)	ΔD (mm)	C_{yl} (mm)	K_f (°)	P_{erp} (mm)	R_e (mm)	R_a (mm)	R_z (mm)
Ideal		6.000	0.000	0.000	0.000	0.000	0.000	the smaller, the better	
Expt	6.000	6.167	0.008	0.051	0.029	0.033	0.041	2.909	26.480
Difference		0.167	0.008	0.051	0.029	0.033	0.041		
Expt	5.900	6.080	0.011	0.045	0.018	0.025	0.052	3.509	28.157
Difference		0.080	0.011	0.045	0.018	0.025	0.052		
Expt	5.800	5.966	0.020	0.048	0.036	0.030	0.056	3.821	28.568
Difference		0.034	0.020	0.048	0.036	0.030	0.056		
Expt	5.700	5.899	0.004	0.064	0.014	0.029	0.042	3.678	24.578
Difference		0.101	0.004	0.064	0.014	0.029	0.042		

(2) Optimum processing parameters determined by multi-objective optimization for all hole-quality parameters were $SOD = 2$ mm, $WJP = 2600$ bar, and $AMFR = 250$ g/min when $TS = 10$ mm/min. Drilling holes using these optimum parameters at $CMD = 6.000$ mm, the hole-quality parameters were $D = 6.167$ mm, $\Delta D = 0.008$ mm, $K_f = 0.029°$, $C_{yl} = 0.051$ mm, $P_{erp} = 0.033$ mm, $R_e = 0.041$ mm, $R_a = 2.909$ µm, and $R_z = 26.480$ µm. The quality of drilled holes was overall satisfactory.

(3) The size of holes generated by the AWJD approach was always larger than *CMD*, resulting in large *D*. The approach to making *D* very close to 6.000 mm was to adjust *CMD* to an appropriate value. Using $CMD = 5.800$ mm to drill holes at the optimal levels, the hole-quality parameters were measured as 0.030 mm, 0.048 mm, 5.966 mm, 0.056 mm, 0.036°, 0.020 mm, 3.821 µm, and 28.568 µm for P_{erp}, C_{yl}, D, R_e, K_f, ΔD, R_a, and R_z, respectively.

(4) Machined surface of holes is highly smooth at roughly 40 × magnification of SEM. At high magnification, ploughing marks were observed on the machined surface, showing that ploughing action was one of the main material removal processes. Ploughing traits of abrasives clearly illustrated the drilling direction of AWJ. Broken abrasive particles were found, showing that secondary material removal process occurred. Images at a low resolution indicated that the machined surface of holes at the top was highly smooth compared to that at the bottom section.

As further investigations, pilot holes will be used to improve P_{erp} and C_{yl} of holes. To reduce the hole-making costs, increase the drilling efficiency, and improve the quality of holes, AWJD parameters will be further optimized at higher *TS*.

Author contributions All authors contributed to the study conception and design. Material preparation, data collection and analysis were performed by PhD student Hang Shi and was checked and validated by Khaled Giasin Antigoni Barouni and Zhongyi Zhang. The first draft of the manuscript was written by Hang Shi and all authors commented on all versions of the manuscript. All authors read and approved the final manuscript.

Funding This study received no funding.

Data availability The data used in this study can be requested from the corresponding author.

Code availability Not applicable.

Declarations

Ethics approval Not applicable.

Consent to participate Not applicable.

Consent for publication Not applicable.

Competing interests The authors have no competing interests to declare that are relevant to the content of this article.

References

1. Aamir M, Tolouei-Rad M, Giasin K, Nosrati A (2019) Recent advances in drilling of carbon fiber-reinforced polymers for aerospace applications: a review. Int J Adv Manuf Technol 105:2289–2308. https://doi.org/10.1007/s00170-019-04348-z
2. Giasin K, Dad A, Brousseau E, Pimenov D, Mia M, Morkavuk S, Koklu U (2021) The effects of through tool cryogenic machining on the hole quality in GLARE® fibre metal laminates. J Manuf Process 64(4021):996–1012. https://doi.org/10.1016/j.jmapro.2021.02.010
3. Bonhin EP, David-Müzel S, Alves MCDS, Botelho EC, Ribeiro MV (2021) A review of mechanical drilling on fiber metal laminates. J Compos Mater 55:843–869. https://doi.org/10.1177/0021998320957743
4. Giasin K (2017) Machining fibre metal laminates and Al2024-T3 aluminium alloy (Doctoral dissertation, University of Sheffield). https://etheses.whiterose.ac.uk/16061/1/PhD%20thesis.pdf. Accessed 25/10/2023
5. Giasin K, Gorey G, Byrne C, Sinke J, Brousseau E (2019) Effect of machining parameters and cutting tool coating on hole quality in dry drilling of fibre metal laminates. Compos Struct 212:159–174. https://doi.org/10.1016/j.compstruct.2019.01.023
6. Yuan P, Lai T, Li Y, Han W, Lin M, Zhu Q, Liu Y, Shi Z (2016) The attitude adjustment algorithm in drilling end-effector for aviation. Adv Mech Eng 8:1–9. https://doi.org/10.1177/1687814016629348
7. Koklu U, Morkavuk S, Featherston C, Haddad M, Sanders D, Aamir M, Pimenov DY, Giasin K (2021) The effect of cryogenic machining of S2 glass fibre composite on the hole form and dimensional tolerances. Int J Adv Manuf Technol 115:125–140. https://doi.org/10.1007/s00170-021-07150-y
8. Sinmazçelik T, Avcu E, Bora MÖ, Çoban O (2011) A review: fibre metal laminates, back- ground, bonding types and applied test methods. Mater Design 32:3671–3685. https://doi.org/10.1016/j.matdes.2011.03.011
9. Giasin K, Hodzic A, Phadnis V, Ayvar-Soberanis S (2016) Assessment of cutting forces and hole quality in drilling Al2024 aluminium alloy: experimental and finite element study. Int J Adv Manuf Technol 87:2041–2061. https://doi.org/10.1007/s00170-016-8563-y
10. Ralph WC, Johnson WS, Toivonen P, Makeev A, Newman JC (2006) Effect of various aircraft production drilling procedures on

hole quality. Int J Fatigue 28:943–950. https://doi.org/10.1016/j.ijfatigue.2005.09.009
11. Vigneshwaran S, Uthayakumar M, Arumugaprabu V (2018) Abrasive water jet machining of fiber-reinforced composite materials. J Reinf Plast compos 37:230–237. https://doi.org/10.1177/0731684417740771
12. Reddy VN, Venkatesh B (2019) Optimization of parameters in abrasive water jet machining of glass laminate aluminium reinforced epoxy (GLARE). Materials Today: Proceedings 19:890–894. https://doi.org/10.1016/j.matpr.2019.08.245
13. Sourd X, Giasin K, Zitoune R, Salem M, Lupton C (2022) Multiscale analysis of the damage and contamination in abrasive water jet drilling of GLARE fibre metal laminates. J Manuf Process 84:610–621. https://doi.org/10.1016/j.jmapro.2022.10.023
14. Nouari M, List G, Girot F, Coupard D (2003) Experimental analysis and optimisation of tool wear in dry machining of aluminium alloys. Wear 255:1359–1368. https://doi.org/10.1016/S0043-1648(03)00105-4
15. Nouari M, List G, Girot F, Géhin D (2005) Effect of machining parameters and coating on wear mechanisms in dry drilling of aluminium alloys. Int J Mach Tool Manuf 45:1436–1442. https://doi.org/10.1016/j.ijmachtools.2005.01.026
16. Davoudinejad A, Ashrafi SA, Hamzah RIR, Niazi A (2012) Experimental analysis of wear mechanism and tool life in dry drilling of Al2024. Adv Mater Res 566:217–221. https://doi.org/10.4028/www.scientific.net/AMR.566.217
17. Kurt M, Kaynak Y, Bagci E (2008) Evaluation of drilled hole quality in Al 2024 alloy. Int. J Adv Manuf Technol 37:1051–1060. https://doi.org/10.1007/s00170-007-1049-1
18. Kurt M, Bagci E, Kaynak Y (2009) Application of Taguchi methods in the optimization of cutting parameters for surface finish and hole diameter accuracy in dry drilling processes. Int J Adv Manuf Technol 40:458–469. https://doi.org/10.1007/s00170-007-1368-2
19. Elajrami M, Milouki H, Boukhoulda FB (2013)Effect of drilling parameters on hole quality. Int J Min Metall Mech Eng 1:254–257. http://journalsweb.org/siteadmin/upload/D1013024.pdf. Accessed 25/10/2023
20. Köklü U (2012) Influence of the process parameters and themechanical properties of aluminum alloys on the burr height and the surface roughness in dry drilling. Mater Technol 46:103–108. http://mit.imt.si/izvodi/mit122/koklu.pdf. Accessed 25/10/2023
21. Amini S, Paktinat H, Barani A, Tehran AF (2013) Vibration drilling of Al2024-T6. Mater Manuf Process 28:476–480. https://doi.org/10.1080/10426914.2012.736659
22. Barani A, Amini S, Paktinat H, Tehrani AF (2014) Built-up edge investigation in vibration drilling of Al2024-T6. Ultrasonics 54:1300–1310. https://doi.org/10.1016/j.ultras.2014.01.003
23. Abdelhafeez AM, Soo SL, Aspinwall DK, Dowson A, Arnold D (2015) Burr formation and hole quality when drilling titanium and aluminium alloys. Procedia CIRP 37:230–235. https://doi.org/10.1016/j.procir.2015.08.019
24. Aamir M, Tolouei-Rad M, Giasin K, Vafadar A, Koklu U, Keeble W (2021) Evaluation of the surface defects and dimensional tolerances in multi-hole drilling of AA5083, AA6061, and AA2024. Appl Sci 11:4285. https://doi.org/10.3390/app11094285
25. Cenac F, Zitoune R, Collombet F, Deleris M (2015) Abrasive water-jet milling of aero- nautic aluminum 2024–T3. Proc IMechE Part L: J Mater 229:29–37. https://doi.org/10.1177/1464420713499288
26. Natarajan Y, Murugesan PK, Mohan M, Khan SALA (2020) Abrasive water jet machining process: A state of art of review. J Manuf Process 49:271–322. https://doi.org/10.1016/j.jmapro.2019.11.030
27. Orbanic H, Junkar M (2004) An experimental study of drilling small and deep blind holes with an abrasive water jet. Proc IMechE Part B: J Eng Manuf 218:503–508. https://doi.org/10.1177/095440540421800504
28. Akkurt A (2009) The effect of material type and plate thickness on drilling time of abrasive water jet drilling process. Mater Des 30:810–815. https://doi.org/10.1016/j.matdes.2008.05.049
29. Nyaboro J, Ahmed M, El-Hofy H, El-Hofy M (2021) Experimental and numerical investigation of the abrasive waterjet machining of aluminum-7075-T6 for aerospace applications. Adv Manuf 9:286–303. https://doi.org/10.1007/s40436-020-00338-7
30. Abdul Lathif SK, Yeswanth IVS, Srinivasulu M, Mani Prasad N (2018) An experimental study and parametric optimization of AWJC on aluminium 7075 alloy. Int J Mech Prod Eng Res Dev 8:667–678. https://doi.org/10.13140/RG.2.2.12867.91688
31. Tekaüt İ (2019) A study on the effect of traverse speed on geometric tolerances in abrasive waterjet drilling of Aa7075 aluminium alloy. Çukurova Univ J Fac Eng Archit 34:1–8. https://dergipark.org.tr/en/download/article-file/790006. Accessed 25/10/2023
32. Ravi RR, Srinivasu DS (2023) A comprehensive parametric study on abrasive waterjet trepanning of Al-6061 alloy. Mate Manuf Process 38(12):1472–94. https://doi.org/10.1080/10426914.2022.2149791
33. Li M, Huang M, Chen Y, Kai W, Yang X (2019) Experimental study on hole characteristics and surface integrity following abrasive waterjet drilling of Ti6Al4V/CFRP hybrid stacks. J Adv Manuf Technol 104:4779–4789. https://doi.org/10.1007/s00170-019-04334-5
34. Dhakal HN, Ismail SO, Ojo SO, Paggi M, Smith JR (2018) Abrasive water jet drilling of advanced sustainable bio-fibre-reinforced polymer/hybrid composites: a compre- hensive analysis of machining-induced damage responses. Int J Adv Manuf Technol 99:2833–2847. https://doi.org/10.1007/s00170-018-2670-x
35. Karataş MA, Motorcu AR, Gökkaya H (2020) Optimization of machining parameters for kerf angle and roundness error in abrasive water jet drilling of CFRP composites with different fiber orientation angles. J Braz Soc Mech Sci Eng 42:173. https://doi.org/10.1007/s40430-020-2261-2
36. Meral G, Sarıkaya M, Mia M, Dilipak H, Şeker U, Gupta MK (2019) Multi-objective optimization of surface roughness, thrust force, and torque produced by novel drill geometries using Taguchi-based GRA. Int J Adv Manuf Technol 101:1595–1610. https://doi.org/10.1007/s00170-018-3061-z
37. Liu H-T (2007) Hole drilling with abrasive fluidjets. Int J Adv Manuf Technol 32:942–957. https://doi.org/10.1007/s00170-005-0398-x
38. Lenin Raj S, Rajadurai A (2019) Experimental study on deep-hole making in Ti-6Al-4V by abrasive water jet machining. Mater Res Express 6:066532. https://doi.org/10.1088/2053-1591/ab0c35
39. Hlavacek P, Hloch S, Nag A, Petru J, Muller M, Hromasová M, Srníček P (2021) Effect of rotation direction, traverse speed, and abrasive type during the hydroabrasive disintegration of a rotating Ti6Al4V workpiece. Proc IMechE. Part B: J Eng Manuf 235:1848–1860. https://doi.org/10.1177/0954405420971226